Fermilab

Fermi National Accelerator Laboratory
P.O. Box 500 • Batavia, Illinois • 60510

TD - 01 - 032
May 03, 2001

Mechanical Design and Analysis of 2-in-1 Warm Iron Yoke Dipole Magnet: Version-2

Deepak Chichili and Alexander Zlobin

Abstract

The mechanical design and analysis of a 2-in-1 high field dipole magnet with warm-iron yoke and aluminum coil support structure is discussed in this report. A bladder system is used to achieve the required pre-stress in the coil.

1.0 Introduction

The first version of the 2-in-1 shell-type dipole magnet with warm iron yoke was reported at ASC-00[*]. Fig. 1 shows the conceptual design of the mechanical support structure. Freestanding 50 mm thick collars support the coils. Wide keys are used to lock the collars in place. Laminated collars can be arranged alternately along the length of the coil with filler piece in-between. Note that the coils are compressed in the horizontal direction during collaring and on cool down. This helps in attaining the required stress distribution in the coils to compensate Lorentz forces. An insert with lower thermal contraction coefficient than collar material separates the two apertures. On cool down the differential thermal contraction between the collar and insert helps in maintaining the prestress in the coils. Thin stainless steel skin around the collars acts as a helium vessel. Preliminary analysis showed that the required pre-stress to the coils can be attained during cool down with aluminum collars and stainless steel inserts due to the large size and higher thermal contraction of aluminum collars. However it was later discovered that the stiffness of the aluminum collar structure is not sufficient to hold the Lorentz forces. So the collar material was changed to stainless steel and insert and key materials to Nitronic 40.

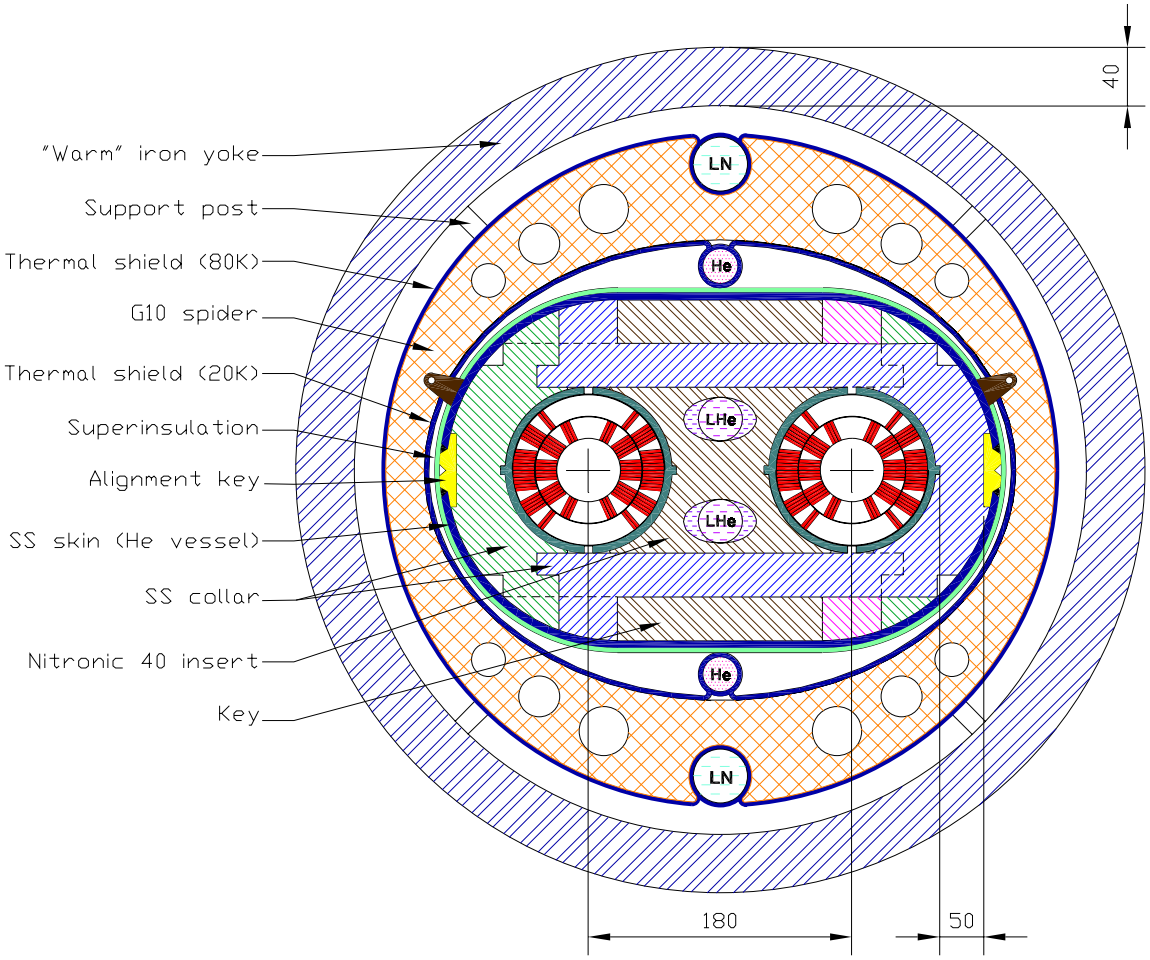

Fig. 1: *Mechanical support structure (VERSION-1) for the "warm" iron yoke design.*

[*] D.R. Chichili, V.V. Kashikhin and A.V. Zlobin, " Mechanical Design and Analysis of 2-in-1 Shell-type Nb_3Sn Dipole Models for VLHC", presented at ASC, Virginia Beech, September 2000.

In order to reduce the quantity of expensive stainless steel collar laminations in Version-1 and the fact that we could increase the vertical diameter of the collar to improve the stiffness prompted us to revisit magnet mechanical design. Fig. 2 shows the conceptual design of the Version-2 mechanical support structure. The design consists of thick laminated aluminum shells and stainless steel spacers held in place using Nitronic-40 inserts. Note that the aluminum shell is still 50 mm wide in the horizontal direction as in Version-1. However the distance from the center of the magnet to the end of shell is set equal both in horizontal and vertical direction (= 180 mm). This will improve the stiffness of the support structure, which will enable us to use aluminum as the shell material in this design. The two bores are separated using stainless steel spacers with some gap at the center of the magnet as shown in the Fig. 2. Coils will be pre-stressed using a bladder system placed in the gap. Once the coils are compressed to the required stress, Nitronic-40 keys will be inserted and the bladders will be removed.

Finite element analysis using ANSYS was carried out to optimize the coil prestress and to minimize the stress in the aluminum shell, stainless steel spacers and Nitronic-40 inserts. It is also important to estimate the magnet cross-section deformation during assembly at room temperature and during excitation at 4.2 K to understand its effect on magnet field quality.

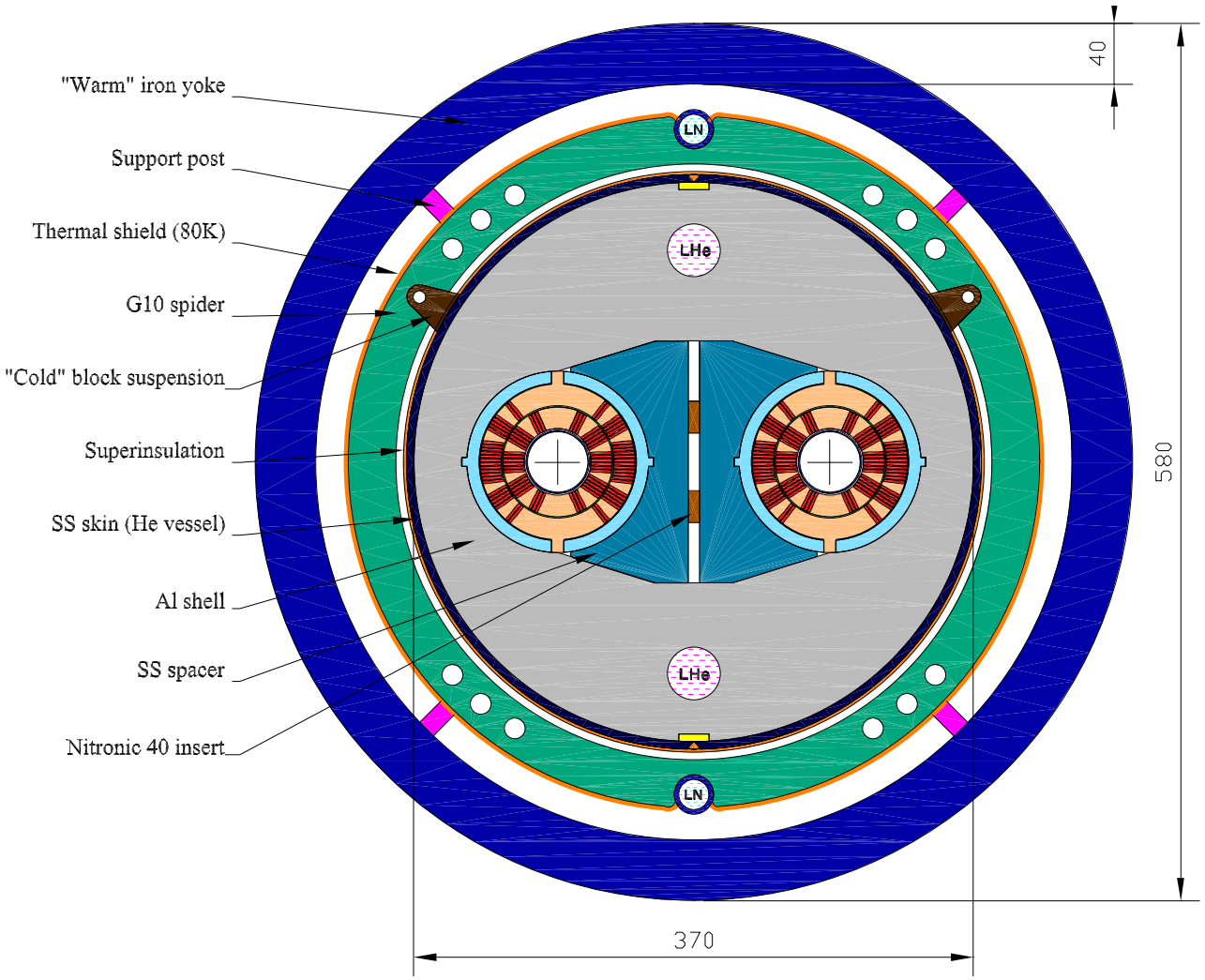

Fig. 2: *Mechanical support structure (VERSION-2) for the "warm" iron yoke design.*

2.0 Finite Element Model

Due to symmetry only quarter section of the magnet was analyzed. The skin not being a structural element in this design was not considered during analysis. As in the Version-1 design, the skin will act only as a helium vessel. Fig. 3 shows the ANSYS model. The areas were meshed with two-dimensional plane stress elements (Plane 42). The contact surface between the aluminum shell and the stainless steel spacer, between the stainless spacer and Nitronic-40 inserts were meshed with CONTACT 48 elements. Having radial interference between the coil and the aluminum shell on one side and the coil and stainless steel spacer on the other side provided the necessary prestress to the coils. This radial interference was obtained through CONTACT 53 elements. A friction coefficient of 0.1 was used for contact elements.

The first step was to evaluate the Lorentz force distribution in the coils at 12 T. Note that the same mesh for the coil will be used for magnetic and mechanical analysis so that the nodal forces can be easily applied.

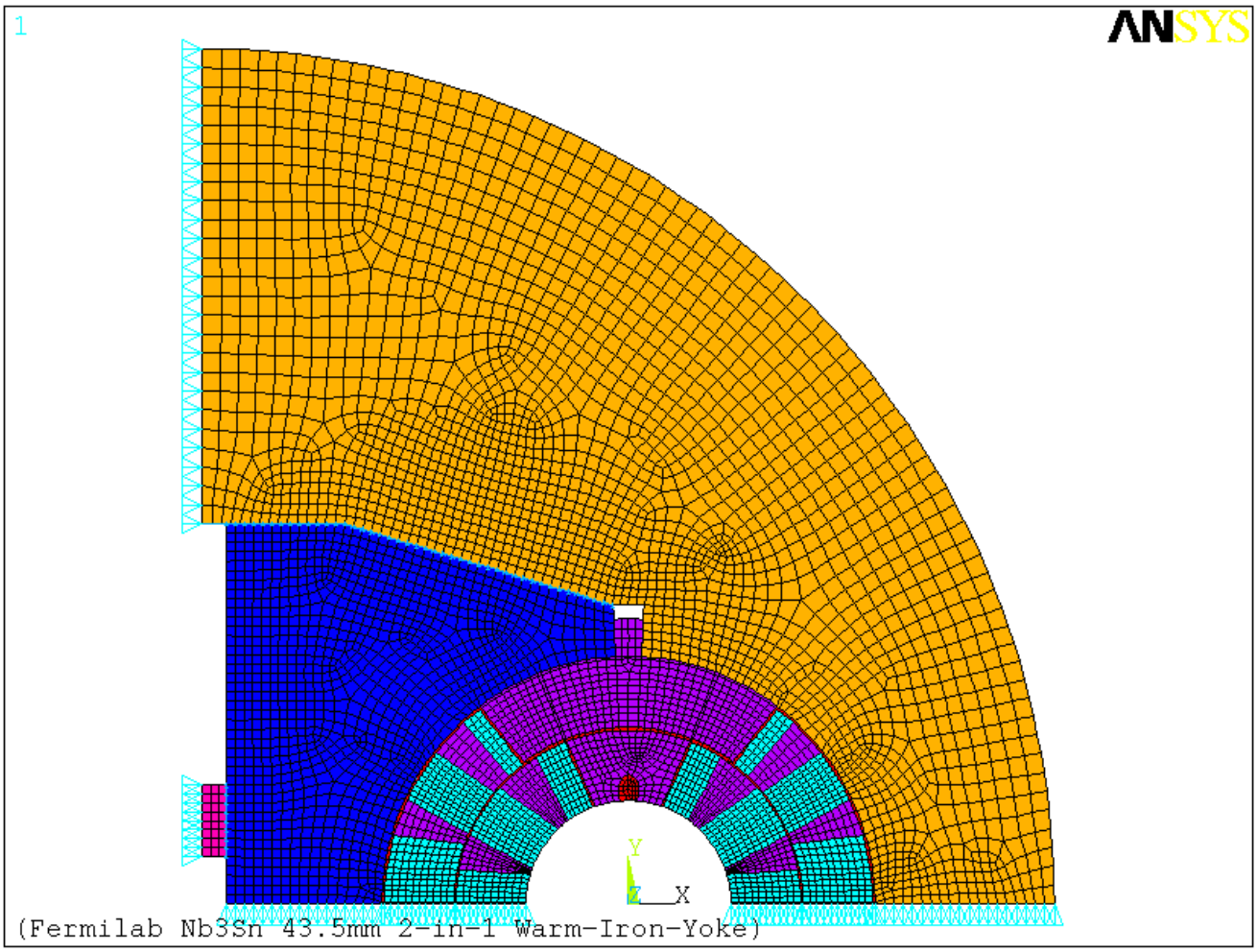

Fig 3: *ANSYS model of the mechanical support structure of Version-2 warm iron yoke design.*

2.1 Lorentz Forces

A quadratic mesh was used in all coil blocks and wedges. Inside each block of the inner layer, the number of elements in azimuthal direction is equal to the number of turns. Each coil block is assumed to have a uniform current distribution and the corresponding current density was computed from the current in each cable times the number of turns in that block. Permeability of iron as a function of magnetic field was used in the analysis. Fig. 4 shows the Lorentz force distribution in the cross-section of the coil at a nominal field of 12 T.

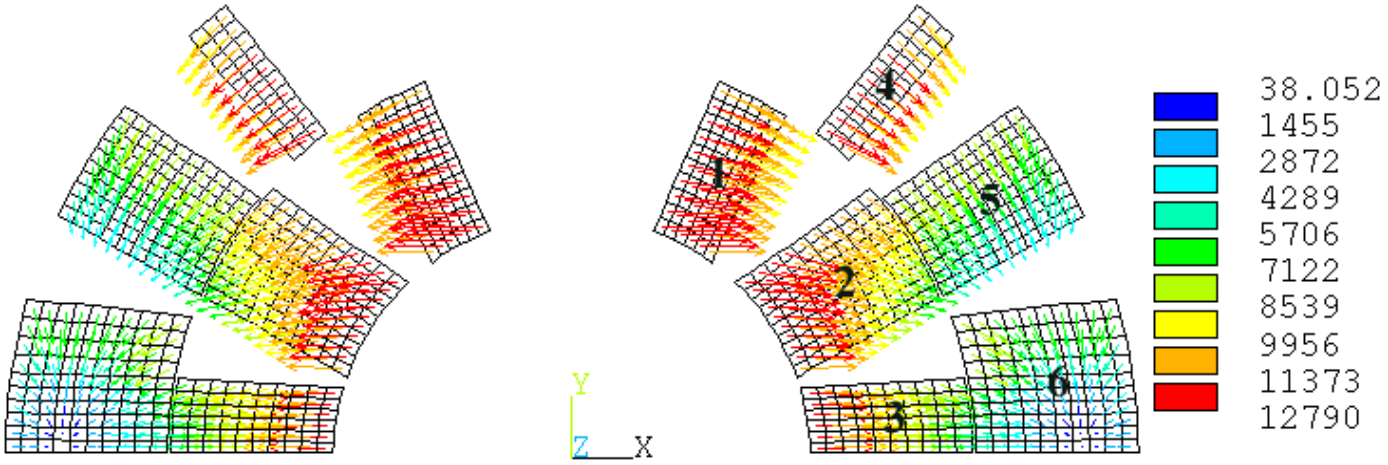

Fig. 4: *Lorentz force distribution in the coil cross-section*.

The Cartesian and Polar components of the Lorentz forces for both the quadrants of the coil are given in Table I.

TABLE I
LORENTZ FORCES IN EACH QUADRANT OF THE COIL AT NOMINAL FIELD

Method	Force	Unit	Left Quadrant	Right Quadrant
ANSYS	F_r	KN/m	1460.6	1458.9
	F_θ		2583.9	-2580.4
	F_x		-2818.3	2815.0
	F_y		-1316.3	-1313.0
OPERA	F_x	KN/m	-2766.0	2762.0
	F_y		-1318.0	-1312.0

2.2 Material Properties

Table II lists the properties of the different materials used in the model. Thermo-mechanical properties were measured using epoxy impregnated Nb_3Sn ten-stack samples. The composite exhibited non-linear behavior during the first loading cycle and a linear behavior with higher stiffness for the successive

loading cycles. These effects were observed both at room temperature and at 4.2 K. Data presented for coil properties in Table II corresponds to the linear behavior during cyclic loading.

TABLE II
THERMO-MECHANICAL PROPERTIES OF MATERIALS USED IN THE ANALYSIS

Material	E (300 K) GPa	E (4.2 K) GPa	α 10^5 K^{-1}
Coil - Azimuthal	38	38	1.21
Coil - Radial	44	55	0.90
Insulation	14	14	2.58
Aluminum Bronze	120	150	1.08
7075 – T651 Aluminum	70	82	1.47
Nitronic – 40	210	225	0.90
Stainless Steel	210	225	1.03

2.3 Analysis Results

The radial interference between the coil and support structure (aluminum shell and the stainless steel spacer) determines the amount of prestress in the coils. Typically this is achieved during production through oversize in coil outer diameter and then compressing the whole structure using the bladder system before inserting the keys. The goal of this analysis was to find an optimum interference between the coil and the support structure.

The acceptable solution should meet the following criteria:

1. The peak stress in the coil should not exceed 150 MPa at all stages of the magnet operation.
2. The coil assembly should be under compression at peak field to ensure that coils do not unload.
3. The maximum stress in the support structures should not exceed the yield stress of the material.

After several iterations, the optimum radial interference between the coil and the aluminum shell was found to be 0.05 mm and between coil and the stainless steel spacer to be 0.15 mm. Fig. 5 shows the azimuthal stress distribution in the coil at room temperature after assembly, at 4.2 K, 0 T and at 4.2 K, 12 T. The stress distribution is asymmetric between the left and right quadrants of the coil at room temperature. This is because the stiffness of the support structures is different for left and right quadrants. However the radial interference between the support structure and the coil for left and right quadrants were chosen such that on cool down, the stress distribution becomes more symmetric in both the quadrants. Note that on cool down, the peak stress in the coil increases from 82 MPa to 133 MPa due to differential thermal contraction between the coil, aluminum shell and stainless steel spacer. The location of the peak stress both at room temperature and on cool down is at the inner layer pole region. On excitation, azimuthal Lorentz forces decrease the stress in the pole region and the location of the peak stress moves to the inner layer mid-plane due to radial Lorentz forces. Table 3 lists the average azimuthal stress values in the inner and outer coil pole and mid-plane regions during various stages of the magnet operation.

Stages	Mean Azimuthal Stress, MPa			
	Inner layer		Outer Layer	
	Pole	Mid-Plane	Pole	Mid-Plane
293 K	66 / 57	45 / 39	51 / 39	66 / 39
4.2 K, 0 T	118	68	75 / 82	89 / 82
4.2 K, 12 T	9	136	54 / 47	122

Table 3: *Average azimuthal stress in the coil. The two values given in some of the columns represent the stress in Left Quadrant / Right Quadrant. Single values represent that they are same in both the quadrants.*

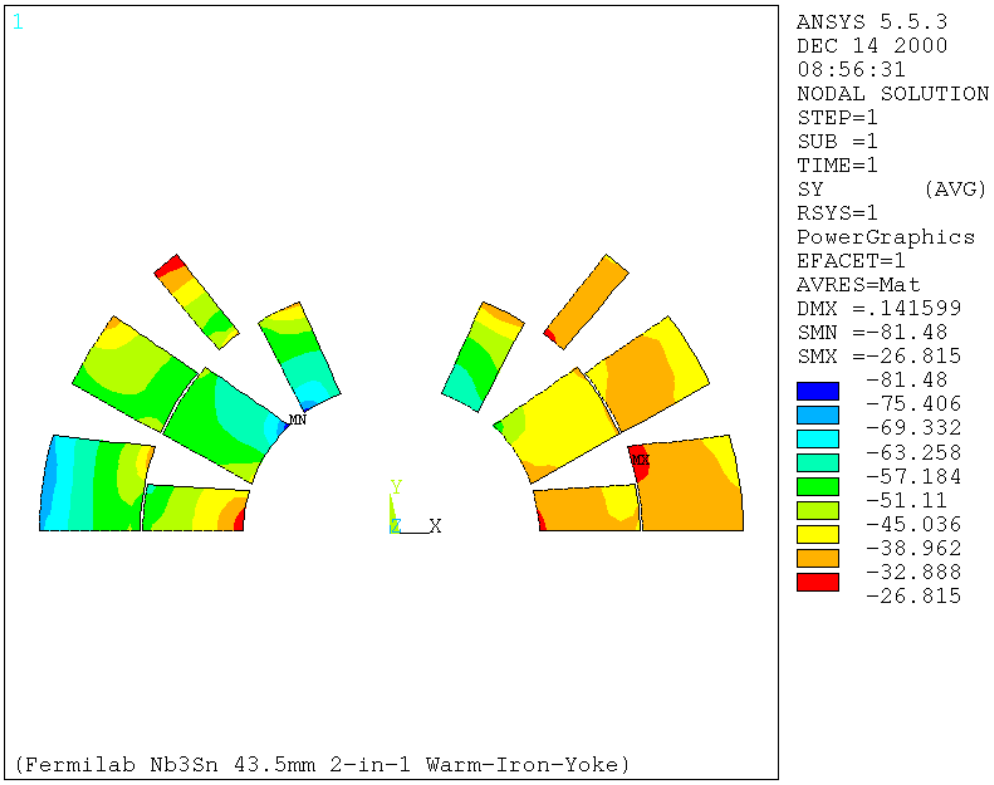

Fig. 5 (a): *Azimithal stress distribution in the coil at room temperature.*

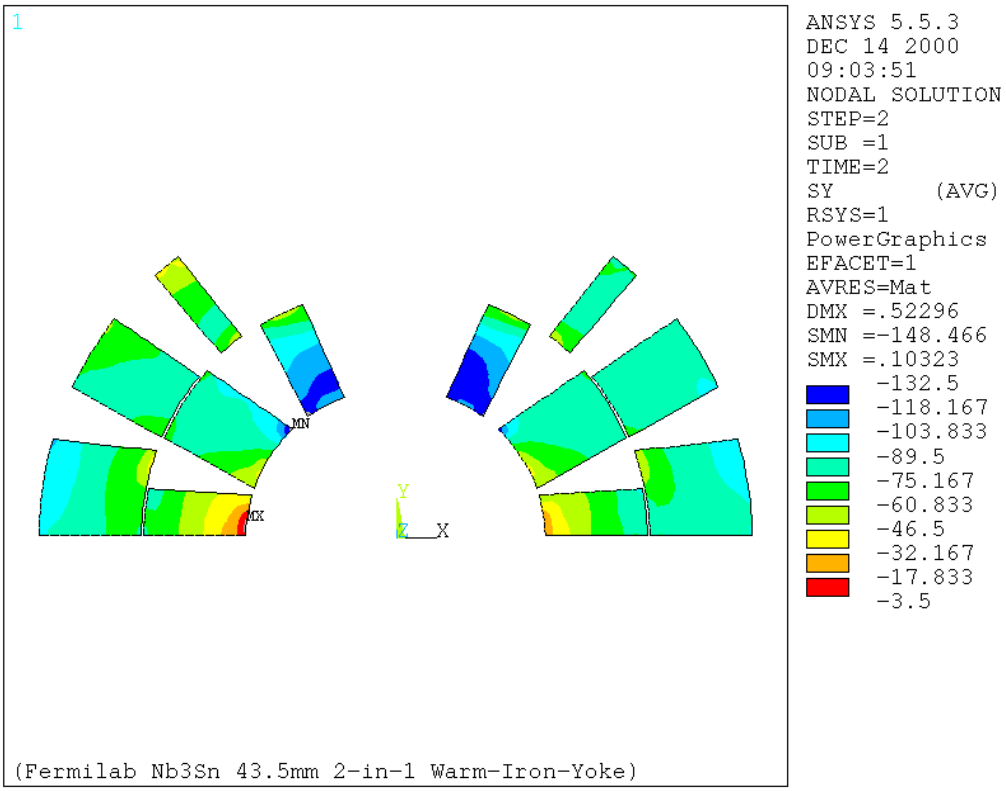

Fig. 5 (b): *Azimithal stress distribution in the coil at 4.2 K, 0 T.*

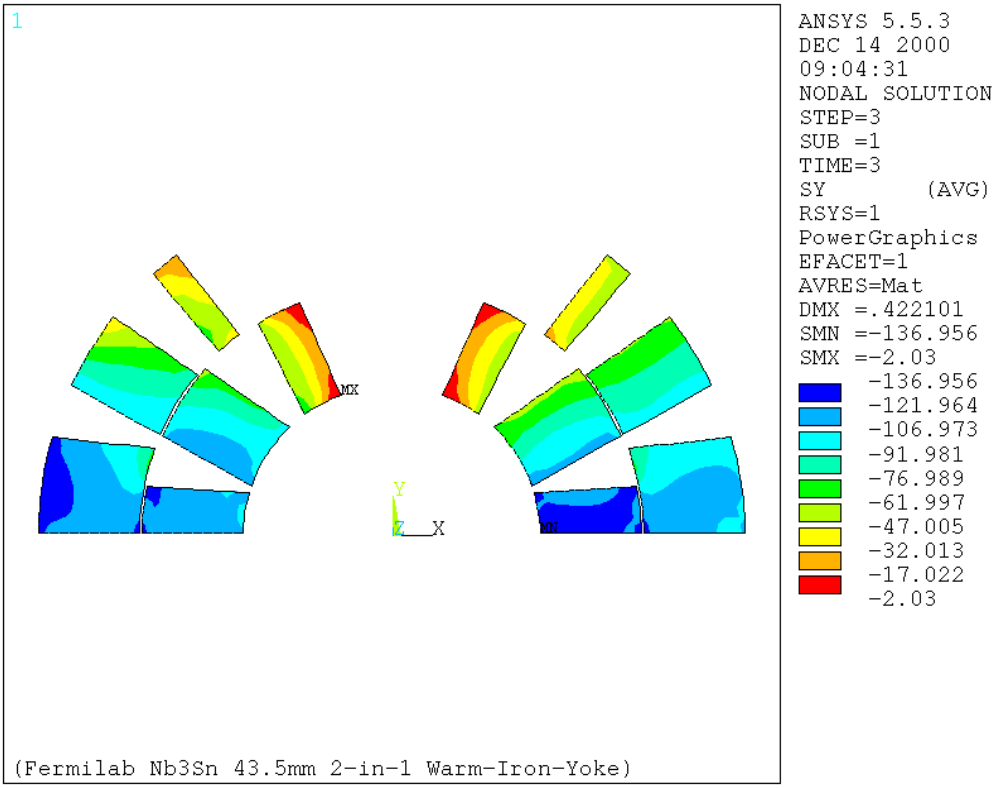

Fig. 5 (c): *Azimithal stress distribution in the coil at 4.2 K, 12 T.*

The Von-Mises stress distribution in the coil support structure at various stages of the magnet operation is shown in Fig. 6. The peak stress in the aluminum shell and in the SS spacer at 293 K, 4.2 K, 0 T and 4.2 K, 12 T is listed in Table 4. The yield stress for 7075-T651 aluminum and 304 stainless steel is about 275 MPa and 300 MPa respectively at room temperature.

Stages	Aluminum Shell, MPa		SS Spacer, MPa	
	Mid-Plane	Pole	Mid-Plane	Pole
293 K	106	71	250	250
4.2 K, 0 T	195	145	340	244
4.2 K, 12 T	222	145	333	185

Table 4: *Peak equivalent stress in the coil support structure. Note that the stress-concentration near the SS spacer/aluminum shell interaction is neglected.*

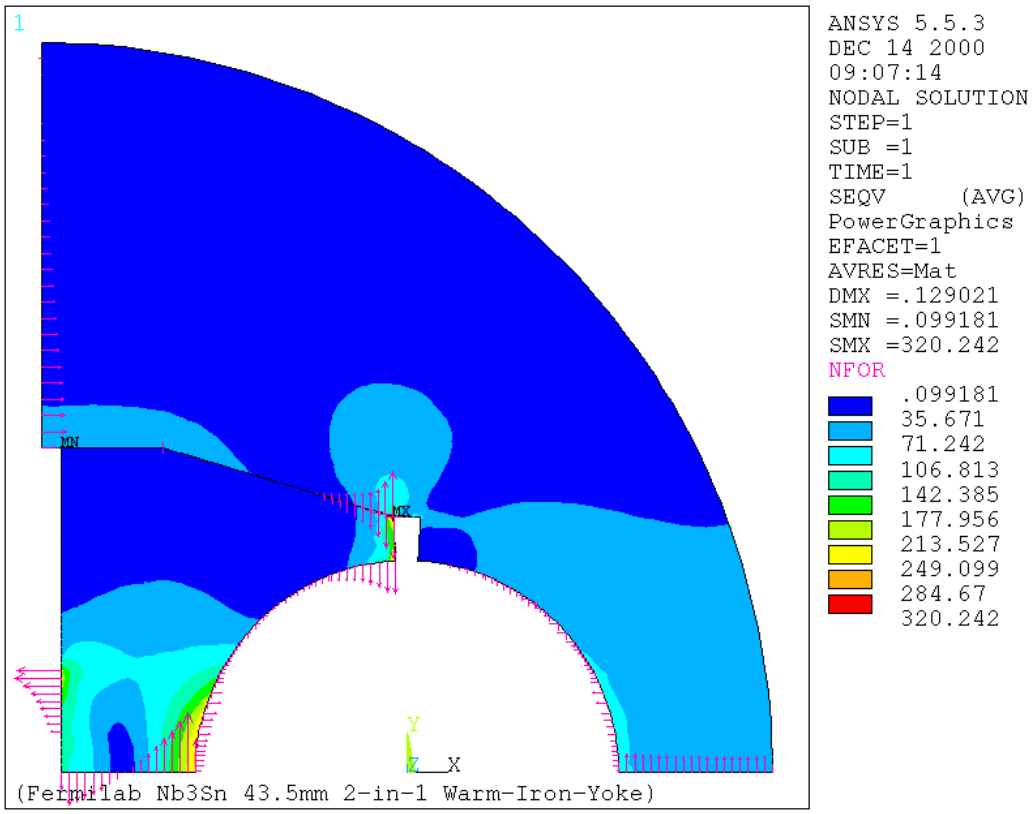

Fig. 6 (a): *Von-Mises stress distribution in the coil support structure at room temperature.*

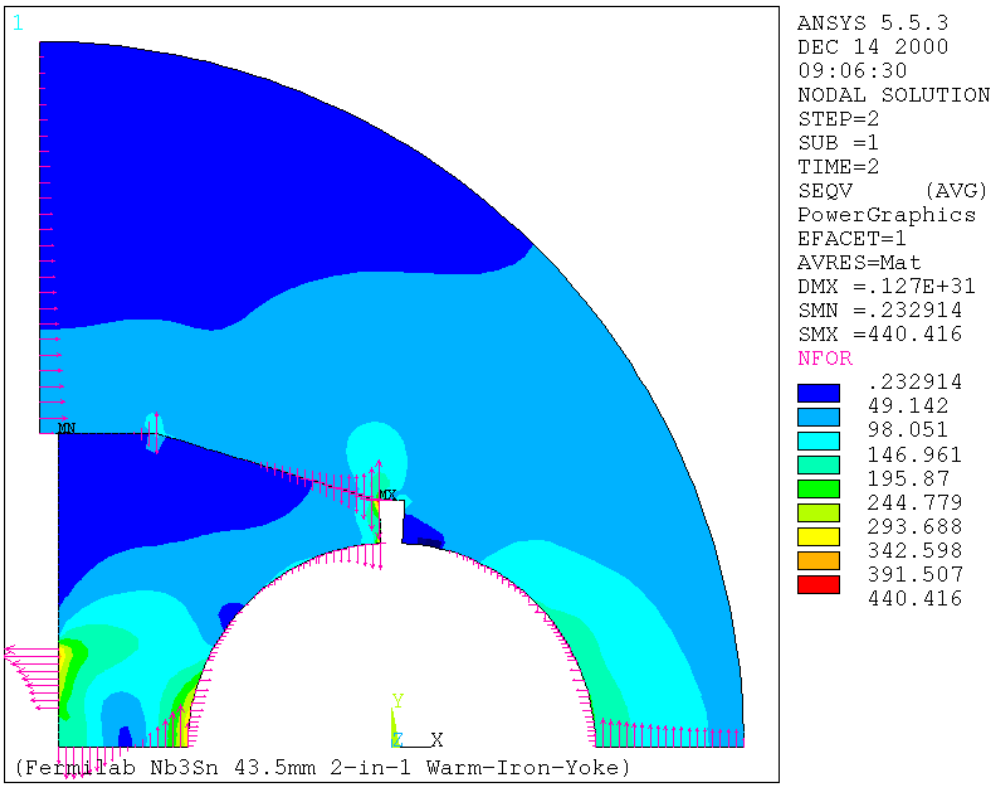

Fig. 6 (b): *Von-Mises stress distribution in the coil support structure at 4.2 K, 0 T.*

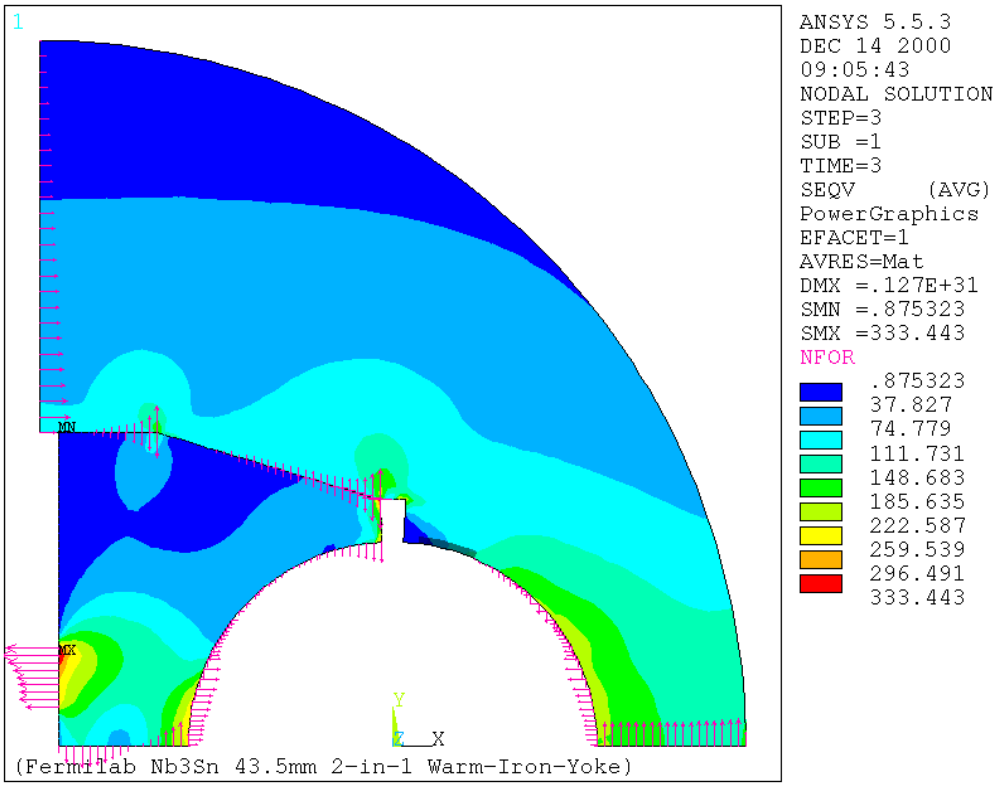

Fig. 6 (c): *Von-Mises stress distribution in the coil support structure at 4.2 K, 12 T.*

In the previous analysis stainless steel was used as the spacer material. To further decrease the cost of the support structure, feasibility study was done to check if aluminum could be used as a spacer material. To simplify the analysis, interferences between the coil and the support structure were set to zero. The whole assembly was first cooled down to 4.2 K and then Lorentz forces were applied. Fig. 7 shows azimuthal stress distribution in the coil at 4.2 K, 0 T and at 4.2 K, 12 T. For comparison, Fig. 8 shows the stress distribution in the coil with stainless steel spacer. On cool down, the amount of pre-stress in the coil is same with both aluminum spacer and SS spacer. However the stress distribution in the coil with aluminum spacer is asymmetric between left and right quadrants, whereas with stainless steel spacer, the distribution is quite symmetric. On excitation, the peak tensile stress with aluminum spacer is 56 MPa more than that of with SS spacer. This could be due to the fact that SS spacer offers better support to the outer shell than the aluminum spacer under Lorentz forces. Hence for this design SS spacer works better.

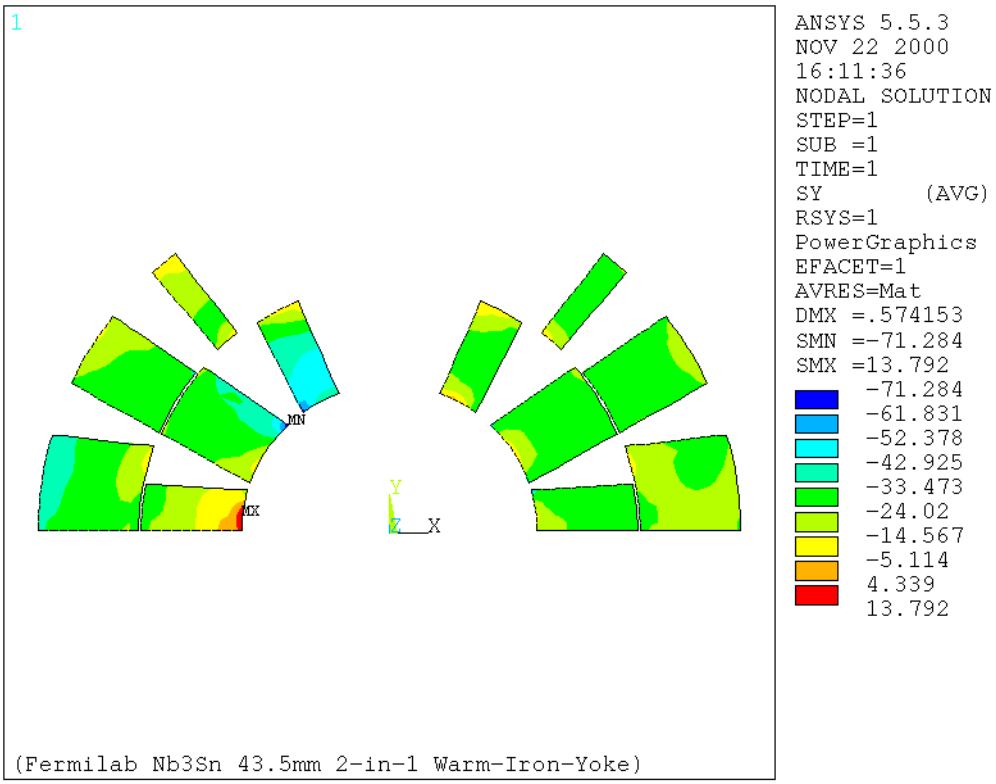

Fig. 7 (a): *Azimuthal stress distribution in the coil at 4.2 K with aluminum spacer.*

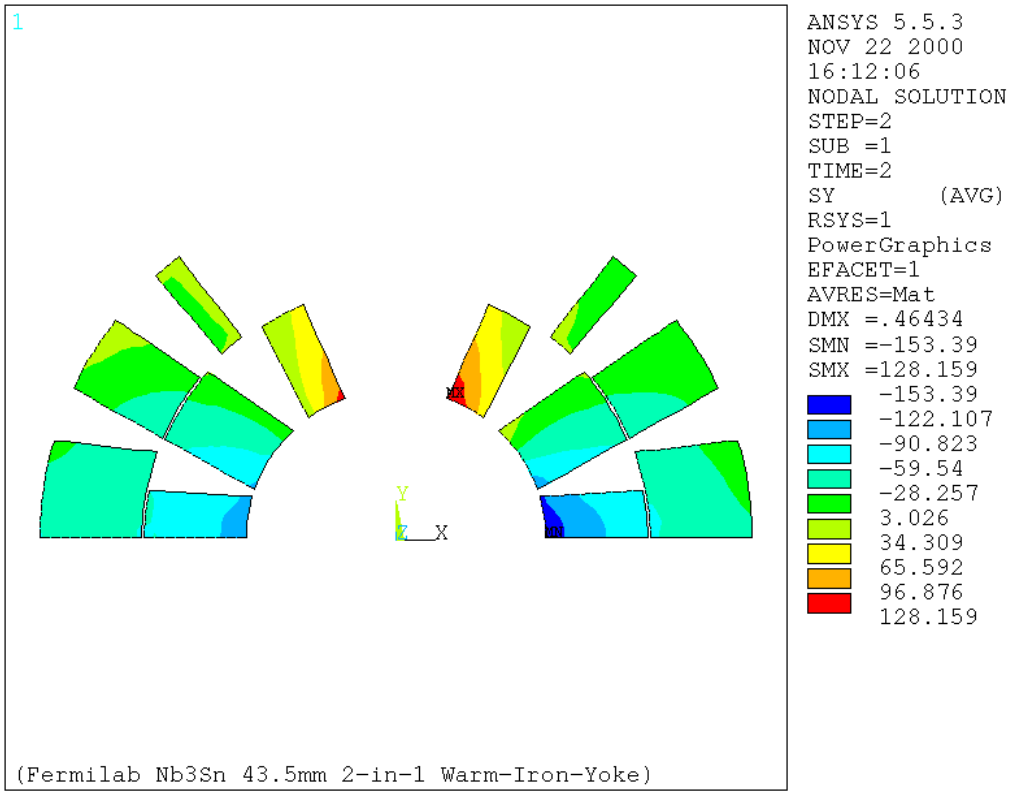

Fig. 7 (b): *Azimuthal stress distribution in the coil at 4.2 K, 12 T with aluminum spacer.*

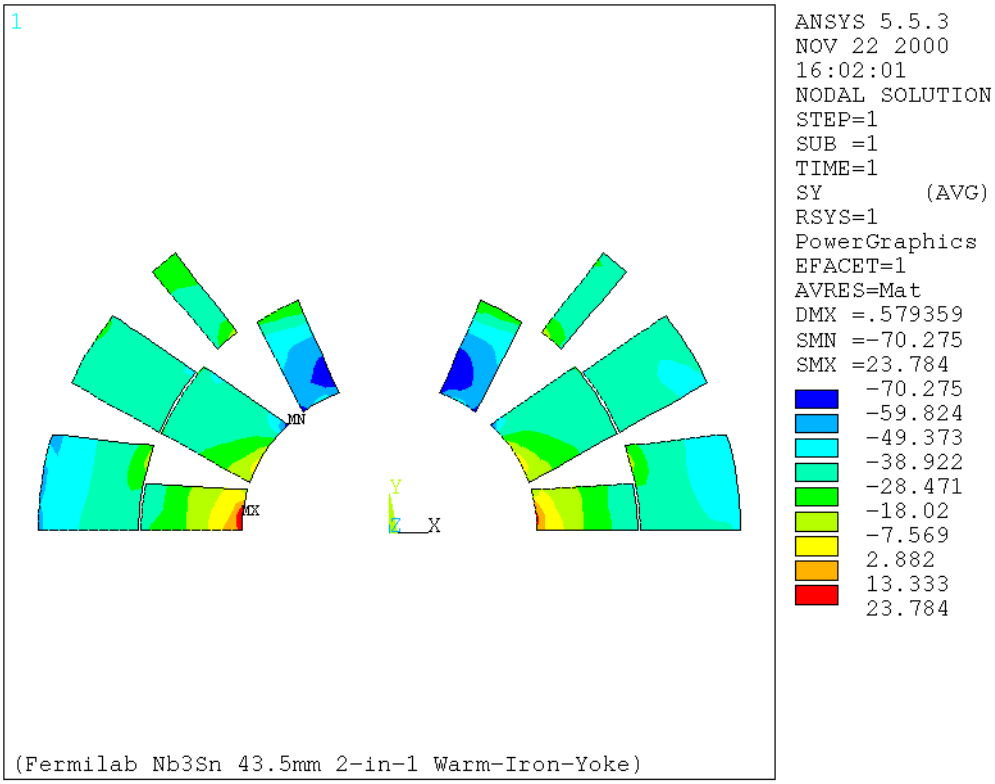

Fig 8 (a): *Azimuthal stress distribution in the coil at 4.2 K with SS spacer.*

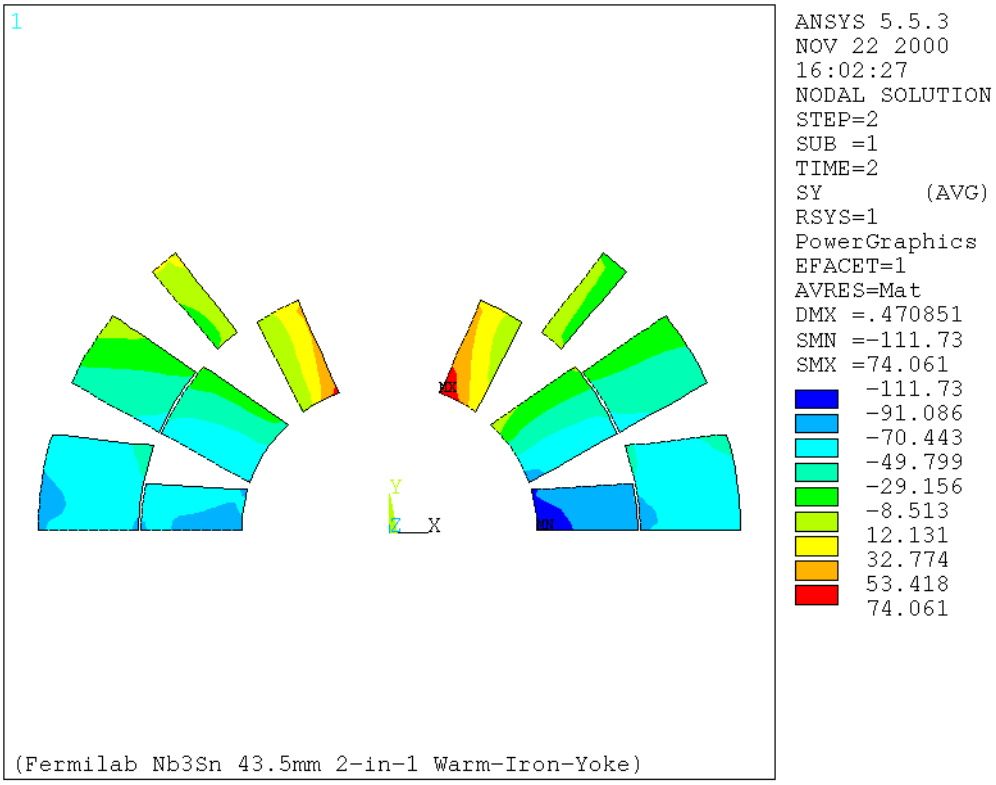

Fig 8 (b): *Azimuthal stress distribution in the coil at 4.2 K, 12 T with SS spacer.*

3.0 Conclusions

A mechanical support structure with outer aluminum shell and stainless steel spacers was developed. The version-2 design reduces the weight as well as the cost of the total magnet cold mass compared to version-1.

A third version of the mechanical design, which will use aluminum laminations with two bores for sliding through the coil assemblies has already been proposed. In this design each layer of the lamination will provide pre-stress only to one side of the coil in each bore. The gap between the shell and the other side of the coil will aide in sliding the laminations. By alternating the shells, the pre-stress will be distributed to the entire length of the coil. A detailed FEA analysis for this design will be reported in a later technical note.